https://doi.org/10.5194/egusphere-2026-3925
Preprint. Discussion started: 16 July 2026

Dust emission, loading, and deposition throughout the Phanerozoic simulated by CESM1.2 coupled with BIOME4

Qi Cui[1], Qifan Lin[1], Jiaqi Guo[1], Yonggang Liu[1*], Yue Liu[1], Xiujuan Bao[1,2], Xiang Li[1,3], Zhibo Li[1,4], Haoyue Zuo[1], Shuai Yuan[1], Yihui Chen[1,5], Shiyan Zhang[1,6], Jian Zhang[1,7], Yongyun Hu[1]

[1]Laboratory for Climate and Ocean-Atmosphere Studies, Department of Atmospheric and Oceanic Sciences, College of Physics, Peking University, Beijing 100871, China

[2]State Key Laboratory of Lithospheric and Environmental Coevolution, Institute of Geology and Geophysics, Chinese Academy of Sciences, Beijing, China

[3]Division of Earth and Climate Sciences, Nicholas School of the Environment, Duke University, Durham, NC, USA.

[4]Department of Earth Sciences, University of Gothenburg, Gothenburg, Sweden

[5]National Satellite Meteorological Center, China Meteorological Administration, Beijing 100081, China

[6]Key Laboratory of Agricultural and Forestry Biosecurity, College of Plant Protection, Nanjing Agricultural University, Nanjing, China.

[7]Key Laboratory of Tibetan Plateau Earth System, Environment and Resources (TPESER), Institute of Tibetan Plateau Research, Chinese Academy of Sciences, Beijing, China.

Correspondence to: Yonggang Liu (ygliu@pku.edu.cn)

Abstract. Atmospheric dust plays a critical role in Earth's climate system and marine biogeochemistry, but how dust varied during the Phanerozoic is still unclear. Here, we simulate the global dust cycle and its climatic impacts during the whole Phanerozoic using an Earth system model with interactive dust. Our results show that the colonization of land by plants near the end of the Silurian caused a fundamental reorganization of the global dust emission, driving a transition from an uninhibited, highly intense dust cycle to one limited largely to unvegetated subtropical regions. Since 410 Ma, subtropical land area and continental fragmentation have acted as the primary controls on dust emissions. Crucially, while total ocean dust deposition broadly follows global emission trends, the oceanic fraction of dust deposition is strongly regulated by paleogeography; more fragmented continental configurations allow dust to be transported more efficiently to the ocean. By comparing the result of dynamically active dust experiments against that of globally uniform prescribed dust experiments, we explicitly isolate the spatiotemporally heterogeneous radiative forcing induced by interactive dust cycles. The uniform dust assumption misrepresents land surface climate, underestimating dust-induced cooling during vegetation-free intervals but overestimating it after plant colonization. Although the first-order temperature response is driven by shortwave radiative attenuation, the final regional response is strongly modulated by localized feedbacks, including snow–albedo, adjustments of cloud and ocean circulation. Overall, this study underscores that deep-time dust is not merely a passive aerosol tracer but an active component of the coupled Earth system that tightly links paleogeography, terrestrial vegetation, marine biogeochemistry, and climate evolution. The modelled dust distribution compares well with the geological records in general but systematically underestimating the dust emission region since 100 Ma, probably because of the overestimation of vegetation by the model

https://doi.org/10.5194/egusphere-2026-3925
Preprint. Discussion started: 16 July 2026

when the fragmentation of continents is high. The present-day dust emission and atmospheric dust loading may be the highest over the past 200 Ma, mainly due to its large subtropical land area.

1. Introduction

Dust, a type of natural aerosol predominantly sourced from arid and semi-arid regions, plays an important role in the climate system and ecosystems. It affects Earth's radiative processes through direct and indirect radiative effects (Atkinson et al., 2013; Huang et al., 2014; Miller & Tegen, 1998), and participates in the cloud and precipitation processes (Andreae & Rosenfeld, 2008; Kushta et al., 2014; Sakaeda et al., 2011). When deposited on the surface, dust may alter surface albedo, especially when there is snow and ice (Krinner et al., 2006; Shi et al., 2019b), and can even have profound impacts on surface morphology (Guo et al., 2001). Additionally, as a key source of trace nutrients, dust deposition influences both terrestrial and marine ecosystems, ultimately affecting the global carbon cycle (Jickells et al., 2005; Okin et al., 2004). On the other hand, dust activity is influenced by climate change (Maher et al., 2010; Zan et al., 2025), and also by the evolution of vegetation and continents on the geological timescale (Lin et al., 2024; Xie et al., 2024). Throughout the Phanerozoic, the Earth experienced shifts between icehouse and greenhouse states (Scotese et al., 2021), the formation and breakup of supercontinents (Scotese & Wright, 2018), and the landing of plants and later evolution (Boyce & Lee, 2017; Salles et al., 2023), all of which could have profoundly influenced dust activity. However, how much the dust source region and thus dust emission, the atmospheric dust loading, and the distribution of dust deposition have changed, and how much they have affected the climate and ecosystem in reverse, are unclear.

Paleo-dust archives, despite their invaluable contribution to understanding historical dust activities, suffer from limited spatial representativeness and uneven temporal and spatial distributions (Cosentino et al., 2024). We will have to rely on climate model simulations to gain a more thorough and systematic understanding of the deep-time dust activity and its impact on climate. A greatly improved understanding of modern dust activity and its responses to changes in temperature, precipitation, vegetation, soil moisture, and wind speed, etc. (Miller et al., 2014; Yang et al., 2019) has enabled the development of decent dust models. These models have been employed to study past dust activity.

Numerous studies have investigated dust-cycle dynamics under past climate states. Shi et al. (2011) used the atmosphere model, CAM3, to explore dust activities during the Pliocene-Pleistocene and the Last Glacial Maximum (LGM), investigating the impacts of the Tibetan Plateau uplift on the dust cycle. Using an atmosphere-ocean general circulation model, CCSM3, Soreghan et al. (2015) simulated that during the Permo-Carboniferous glaciation. They found that the primary dust sources were the subtropical deserts of Pangaea, and that colder climates expanded the extent of these source regions. Liu et al. (2020) employed a new version of CCSM, CESM1.2.2, to simulate the Precambrian dust cycles, revealing enormous dust emission compared to present-day levels due to the absence of vegetation on land. Lin et al. (2024), also using CESM1.2.2, investigated

https://doi.org/10.5194/egusphere-2026-3925
Preprint. Discussion started: 16 July 2026

the dust activities during three typical periods (240 Ma, 130 Ma, and 80 Ma) of the Phanerozoic. These three periods not only differ fundamentally in continental configuration, but also in climate, and their results show that the continental configuration controls the amount of dust emission and loading, with climate and vegetation evolution having negligible influence. Collectively, these studies have substantially improved our understanding of past dust cycles. Nevertheless, they are largely restricted to individual geological intervals or selected time slices, leaving the long-term evolution of dust activity across the Phanerozoic insufficiently explored. Xie et al. (2024) utilized a new offline dust emission model, DUSTY1.0, driven by the climate fields obtained from an AOGCM, HadCM3L, to simulate for the first time the long-term evolution of dust emission over the entire Phanerozoic. However, their study did not account for dust transport, deposition, or its climate effects. A comprehensive, quantitative assessment of dust fields—including emissions, loading, deposition—and their climatic impacts across the Phanerozoic is still lacking.

Building on these previous works, this study aims to provide a comprehensive simulation of the global dust activities throughout the Phanerozoic. Based on the simulation results, the influences of continental tectonics, climate changes, and terrestrial vegetation changes on the dust activities will be systematically analyzed. In addition, how the dust has influenced the climate is also examined. The paper is organized as follows. Section 2 describes the model framework and experimental design. Section 3 presents the main results, beginning with the long-term evolution and controlling factors of dust emission, followed by the evolution of dust deposition and atmospheric loading, and then the climatic impacts of spatiotemporally non-uniform dust relative to that of prescribed uniform dust. Section 4 compares the simulated dust deposition patterns with geological records of aeolian deposits. Section 5 discusses the major uncertainties and limitations, the role of vegetation evolution in regulating the dust cycle, and the climatic effects of dust and their uncertainties. Finally, Section 6 summarizes the main findings and implications of this study.

2. Method

2.1 Climate and vegetation model

In this study, we employ the same model as in Lin et al. (2024), that is, the Community Earth System Model version 1.2.2 (CESM1.2.2), an AOGCM that integrates components for the atmosphere, ocean, land, sea ice, and rivers, all interconnected through a coupler (Hurrell et al., 2013). The atmospheric component (Community Atmosphere Model version 4, CAM4) contains 26 vertical layers and shares the same horizontal resolution (3.75° × 3.75°) with the land components (Community Land Model version 4, CLM4). The ocean (Parallel Ocean Program version 2, POP2) and sea-ice (Community Ice Code version 4, CICE4) components have a nominal 3° irregular horizontal grid. The river transport map (RTM) has a horizontal resolution of 0.5° × 0.5°. These configurations are the same as those in Li et al. (2022) and Lin et al. (2024).

https://doi.org/10.5194/egusphere-2026-3925
Preprint. Discussion started: 16 July 2026

In CAM4, the dust cycle consists of three parts: emission, transport, and deposition (Albani et al., 2014). The emission scheme is based on the Dust Entrainment and Deposition (DEAD) model, in which dust emission is influenced by wind friction velocity, soil moisture, vegetation cover, snow cover, and soil erodibility (Zender et al., 2003). The dust is divided into four size bins (0.1–1.0 μm, 1.0–2.5 μm, 2.5–5.0 μm, and 5.0–10.0 μm), each accounting for 3.8 %, 11 %, 17 %, and 67 % of the total emission mass flux (Neale et al., 2010). The dust transport is simulated using the tracer advection scheme (Neale et al., 2010). Dust deposition occurs via two processes: wet and dry deposition. Wet deposition represents the removal through the convective and large-scale rainfall and snowfall processes, which includes in-cloud precipitation and below-cloud precipitation (Zender et al., 2003). Dry deposition is further classified into gravitational settling and turbulent deposition processes. The model can also partially simulate the climate effects of dust. In this study, only the shortwave direct effect is considered; the longwave radiative effect of dust and the indirect effect of dust through clouds are not considered. The detailed description and setup of this part can be found in Lin et al. (2024).

The built-in vegetation model in the land component (CLM4) of the CESM1.2.2 is a carbon-nitrogen model with dynamic vegetation (CNDV), which tends to generate rather low vegetation coverage (Castillo et al., 2012; Lin et al., 2024). This underestimated vegetation cover will have a substantial impact on dust emission, hence not appropriate for the purpose of this study. Instead, we have chosen to use the BIOME4 model, a coupled biogeographic and biogeochemical model (Kaplan et al., 2003b), which has been successfully applied in numerous paleoclimate simulations (e.g., Albani et al., 2015; Kaplan et al., 2003b). BIOME4 is run in coupled mode with CESM1.2.2 as was done in Lin et al. (2024). A vegetation cover (defined as the sum of the leaf area index and stem area index) threshold of 0.3 m^2/m^2 is set based on observational data. Dust emissions at grids with vegetation cover exceeding this threshold will be completely suppressed (Zender et al., 2003). The CESM1.2.2–BIOME4 coupled framework has been validated to reasonably reproduce the present-day climatological dust cycle (Lin et al., 2024).

2.2 Experimental Setup

The evolution of Phanerozoic dust was obtained in two steps. First, climate and vegetation were simulated using the coupled CESM1.2.2–BIOME4 model in which dust was prescribed to be spatiotemporally uniform, and is thus named as DUST1. This set of experiments was run to quasi-equilibrium. Second, dust emission, transport, and deposition were explicitly simulated using CESM1.2.2 and named as DUST2. These experiments were initialized from the equilibrium state of DUST1 and continued for only 100 years, which is long enough for the dust cycle to equilibrate.

The experiments conducted in DUST1 are very similar to those of Li et al. (2022) except that here the coupled CESM1.2.2–BIOME4 model is used. Li et al. (2022) simulated the climate once every 10 million years for the past 540 million years using the fully coupled CESM1.2.2. Their land-sea mask and surface elevation came from Scotese & Wright (2018). The solar constant decreased at a rate of 0.08 % per 10 million years relative to the present day (Gough, 1981). The atmospheric CO_2

https://doi.org/10.5194/egusphere-2026-3925
Preprint. Discussion started: 16 July 2026

concentration (pCO_2) was adjusted for each time slice (55 in total) to ensure that the simulated global mean surface temperature (GMST) remained within 0.5 °C of that reconstructed by Scotese (2016). We replaced the built-in CNDV vegetation model with BIOME4, and the plant colonization and the emergence of angiosperms and C4 plants (Cerling et al., 1997; Li et al., 2019) are also considered. Specifically, plants are assumed to be absent on land between 540 Ma and 420 Ma; land plants are present between 410 Ma and 110 Ma, but neither angiosperms nor C4 plants are included; angiosperms are included, but C4 plants are absent between 110 Ma and 20 Ma; C4 plants are further included for 10 Ma. It turned out that the newly simulated vegetation induced a large climate change (see Fig. S1 for an example). Therefore, we have to re-tune pCO_2 for each time slice as was done in Li et al. (2022) to ensure the simulated GMST is within 0.5 °C of Scotese's reconstructed GMST (Scotese, 2016) (Fig 1a). In these experiments, the dust cycle was not activated. Not only dust, but also the atmospheric loading of all the other aerosols such as sulfate, soot, sea salt, organic carbon, etc., was set to be uniform, with values the same as the global annual average today. The detailed boundary conditions, including atmospheric CO_2 concentrations and solar radiation, are summarized in Table S1. All simulations were continued for longer than 3500 years until equilibrium was reached, defined by the criterion that the global mean net radiation at the top of the atmosphere (TOA), averaged over the last 100 model years, is within ±0.1 W/m². In all simulations, there are no prescribed ice sheets, except for the 0 Ma simulation, which is performed with the model default present-day ice sheets.

In DUST2, the dust cycle was activated, and the prescribed uniform dust aerosol was removed. These simulations were initialized using the climate states averaged over the last 100 years of the DUST1 runs. The vegetation distribution was fixed to that obtained in DUST1. The soil erodibility is set to be uniformly 0.16, as has been determined by Lin et al. (2024). All external forcings, including the solar constant and atmospheric CO_2 concentration, are inherited from the corresponding DUST1 simulations. The DUST2 simulations were integrated for 100 model years, capturing the relatively fast response of the climate system to the newly activated dust radiative forcing. The key variables, including global dust emission, loading, lifetime, oceanic deposition, and global mean surface temperatures (GMSTs) across the 55 simulations, averaged over the last 40 years of simulations, are provided in Table S1.

3. Results

3.1 Evolution and Controlling Factors of Dust Emission

Over the past 540 million years, global dust emission has exhibited significant fluctuations (Fig. 1b). The dust activities changed fundamentally at the end of the Silurian (Fig. 1b), when the continents started being colonized by land plants. The Phanerozoic Eon is thus divided into two parts, 540 Ma–420 Ma and 420 Ma–0 Ma, and their results will be described separately.

https://doi.org/10.5194/egusphere-2026-3925
Preprint. Discussion started: 16 July 2026

Prior to plant colonization (540 Ma–420 Ma), dust could be generated from nearly all terrestrial surfaces except snow-covered regions (Fig. 2), with dust source regions (defined as regions where dust emission is higher than 1 $g/m^2/yr$; Fig. 3a) accounting for 91% – 99% of the continental area. Both global dust emission (5,400 to 8,200 Tg/yr) and dust loading (37 to 57 Tg/yr) were substantially higher than the 0 Ma levels (2,218 Tg/yr and 23.4 Tg/yr, respectively). Although much larger than the present-day level, the simulated dust emission and loading are much smaller than those simulated for the Neoproterozoic by Liu et al. (2020). This difference may be due to the difference in continental configuration between the two studies: there was much more subtropical land in Liu et al. (2020) than in this study. Although dust can be emitted everywhere, the emission is still strongest within the subtropical region where the soil is dry and the coastal regions of most latitudes where wind speeds exceed those in the continental interior (Fig. S2). The dust emission is relatively low in the continental interior, mainly due to weaker wind stress there.

The fluctuations of global dust emission between 540 Ma and 420 Ma were small in general (Fig. 1b), especially in terms of relative changes, and were driven by multiple factors. The correlation between the time series of global dust source area and dust emission is quite low (0.06; Fig. 3c). This weak correlation indicates that source area alone cannot explain the temporal evolution of dust emission. Instead, changes in near-surface wind stress, soil moisture, and the spatial distribution of erodible land must also play important roles. It is also notable that the dust emission was not impacted by global climate change in a simple way; when GMST decreases from 26.5 °C in 470 Ma to 18.5 °C in 440 Ma (Fig. 1a), the emission changes only slightly from 6750 Tg/yr to 5850 Tg/yr (Fig. 3c), no larger than the changes between 540 Ma and 470 Ma when GMST was very stable. The pronounced increase in global dust emissions at 420 Ma highlights the key role of wind speed. Despite a smaller continental area and dust source area at 420 Ma, total dust emission reached the maximum of the prior-plant-colonization interval (Fig 3b). This was primarily because annual-mean winds in the subtropics—i.e., over the principal dust-source regions—were the strongest at that time (Fig 3b), due to substantial global cooling (Fig. 1a). Despite the high wind speed in subtropical land, the dust emissions during 450–430 Ma were still low, which is likely driven by extensive snow cover during this cold interval, which suppressed dust emission (Fig S3). Overall, prior to plant colonization, global dust emission was primarily controlled by the spatial co-occurrence of strong near-surface winds and erodible land surfaces. Variations in continental area or GMST played a secondary role.

https://doi.org/10.5194/egusphere-2026-3925
Preprint. Discussion started: 16 July 2026

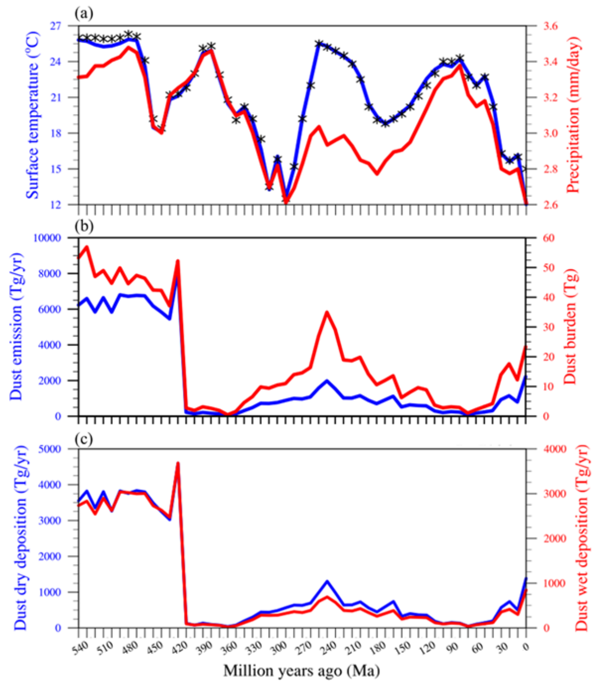

180 **Figure 1.** Simulated annual mean GMSTs and precipitation for the past 540 million years. The black asterisks denote reconstructed GMSTs by Scotese (2016) (a). Global annual-mean atmospheric dust loading and dust emission (b); global annual-mean atmospheric dust dry deposition and wet deposition (c) for the past 540 million years.

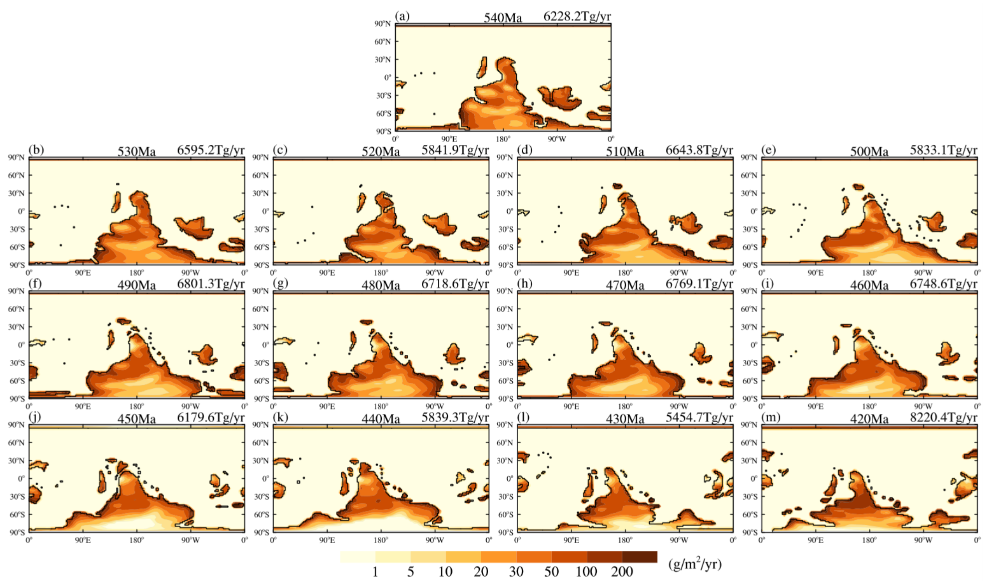

185 **Figure 2.** Annual-mean dust emission (g/m^2/yr) for 540 Ma-420Ma.

After the colonization of plants at around 410 Ma, most land areas lost the ability to emit dust, and dust could only be emitted from unvegetated or sparsely vegetated regions. As a result, compared to periods earlier than 410 Ma, the extent of dust source regions was reduced by nearly an order of magnitude (compare Fig. 3e to Fig. 3a). After plant colonization, dust sources were largely restricted to dry, sparsely vegetated subtropical regions (Figs. 4 and 5). They occurred preferentially over the western and interior parts of continents, whereas the eastern margins were generally wetter under the influence of summer monsoons and thus supported denser vegetation, suppressing dust emission there (Hu et al., 2023). Correspondingly, both dust emission and dust loading decreased substantially, to a range of 57 to 2,218 Tg/yr and 0.5 to 35 Tg/yr, respectively.

The evolution of dust source regions and global emissions since 410 Ma has been primarily controlled by the extent of subtropical land (Fig. 3e, g), validating the mechanism proposed by Lin et al. (2024) and Xie et al. (2024). Under this primary control, modeled global dust emissions exhibited a long-term trajectory: rising from 410 Ma to a peak of 1981.3 Tg/yr at 240 Ma, declining to a minimum of 79.5 Tg/yr at 70 Ma, and recovering to 2217.8 Tg/yr at 0 Ma (Fig. 1b). Other than the subtropical land area, the fragmentation (defined as the ratio of coastline length to land area as in Li et al. (2022)) of continents serves as a vital modulating factor that can override the influence of land area sometimes (Fig 3f). The importance of fragmentation is best seen during the period 110 Ma to 60 Ma, when the subtropical land area was relatively large, yet dust emission remained low. Coincidently, the continental fragmentation during this period is high (Fig. 3f). This high fragmentation allows moisture to penetrate into the continental interior, allowing vegetation to grow (Fig. 5), and the dust source area to contract (Fig. 3f and Fig. 4).

Our simulation shows significantly higher dust emissions before plant colonization but overall lower emissions after plant colonization compared to Xie et al. (2024) (Fig. S4). In the latter, the simulated global dust emission before plant colonization was quite low, even lower than most time periods after plant colonization. They further performed sensitivity tests in which all land areas, except prescribed ice sheets, were treated as non-vegetated prior to 360 Ma. These tests showed that their baseline simulations underestimated early Paleozoic dust emissions, mostly by 5%–30%, and by up to a factor of about two during several emission peaks. However, even after accounting for this correction, their estimated dust emissions before plant colonization remain substantially lower than those simulated in our study. This difference may arise because their sensitivity tests were conducted within an offline dust-emission framework, in which climate, soil moisture, and land-surface conditions did not adjust interactively to the complete absence of vegetation. In our coupled framework, the complete absence of plants leads to a significant reduction in soil moisture through altered hydrological cycles, thereby lowering the threshold for dust generation. Furthermore, during the supercontinent period, the dust emission is lower than the estimations of Xie et al. (2024) (Fig. S4) and dust source regions in our results are also noticeably fewer in the equatorial regions, with virtually no dust emission along the eastern edge of the supercontinent (Figs. 4q-4v). This is because, during the supercontinent period, the vegetation cover along the eastern supercontinent coast is quite good (Figs. 5q-5v), exceeding the dust emission threshold of 0.3, thus effectively suppressing dust emissions in these areas. This also explains the disappearance of dust source areas in

https://doi.org/10.5194/egusphere-2026-3925
Preprint. Discussion started: 16 July 2026

North America in the Middle and Late Cretaceous in our simulation results (Figs. 4aj-ai). Another significant difference between our simulation and Xie et al. (2024) appears in the Cenozoic North African dust region. In our simulation, the North African dust source region does not appear until 30 Ma (Fig. 4am), whereas it already reached a considerable scale around 50 Ma in Xie et al. (2024). This discrepancy may reflect differences in simulated regional hydroclimate and vegetation cover between the two modeling frameworks. In particular, differences in precipitation, soil moisture, and the treatment of vegetation suppression on dust emission could strongly influence the timing and extent of dust-source development.

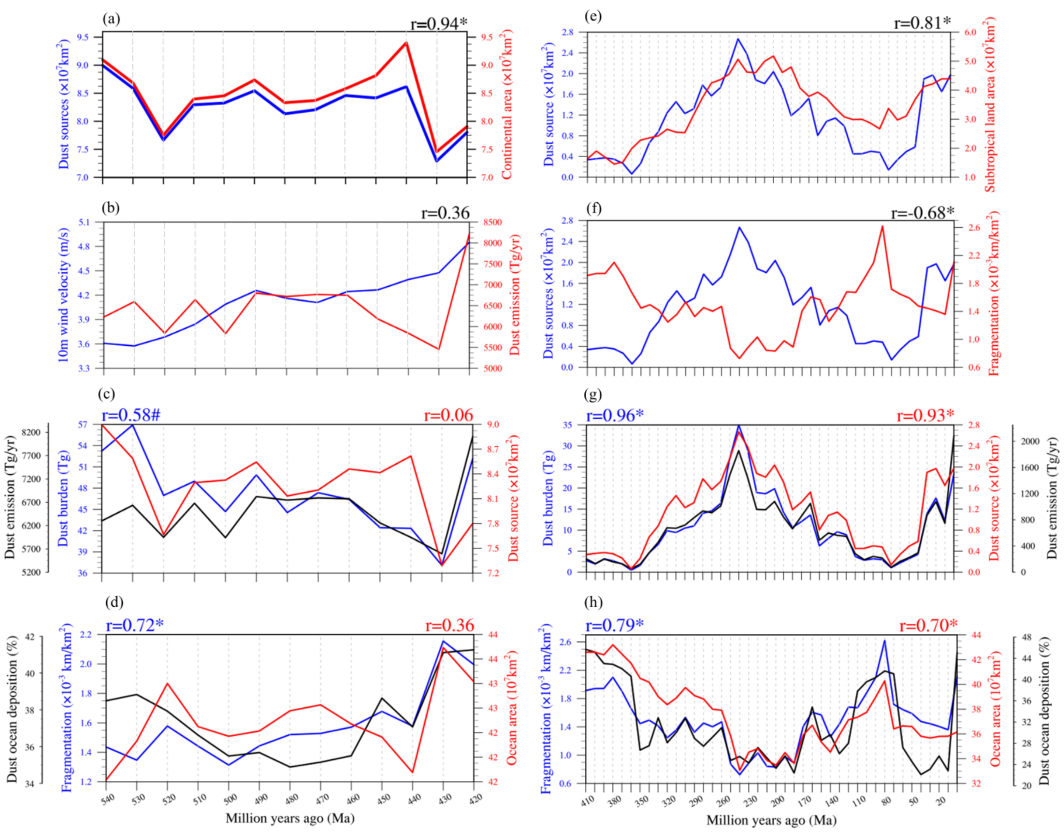

Figure 3. The evolution of annual mean land area and dust source area (a), dust emission and 10 m wind velocity averaged over subtropical land (b) for 540 Ma-420 Ma. The evolution of subtropical land area and dust source area (e); dust source area and land fragmentation (f) for 410 Ma-0 Ma. The upper right corners display the correlation coefficients. The evolution of dust source area, dust emission, and dust burden for 540 Ma-420 Ma (c) and 410 Ma to 0 Ma (g). The upper right and left corners display the correlation coefficients between dust emission and the dust source area, and between dust emission and the dust burden. The evolution of dust ocean deposition ratio, ocean area, and land fragmentation for 540 Ma-420 Ma (d), and for 410 Ma to 0 Ma (h). The upper right and left corners display the correlation coefficients between the dust ocean deposition ratio and the ocean area, and between the dust ocean deposition ratio and the land fragmentation. (*) indicates statistical significance at the 95% confidence level, whereas a hash (#) indicates significance at the 90% confidence level.

https://doi.org/10.5194/egusphere-2026-3925
Preprint. Discussion started: 16 July 2026

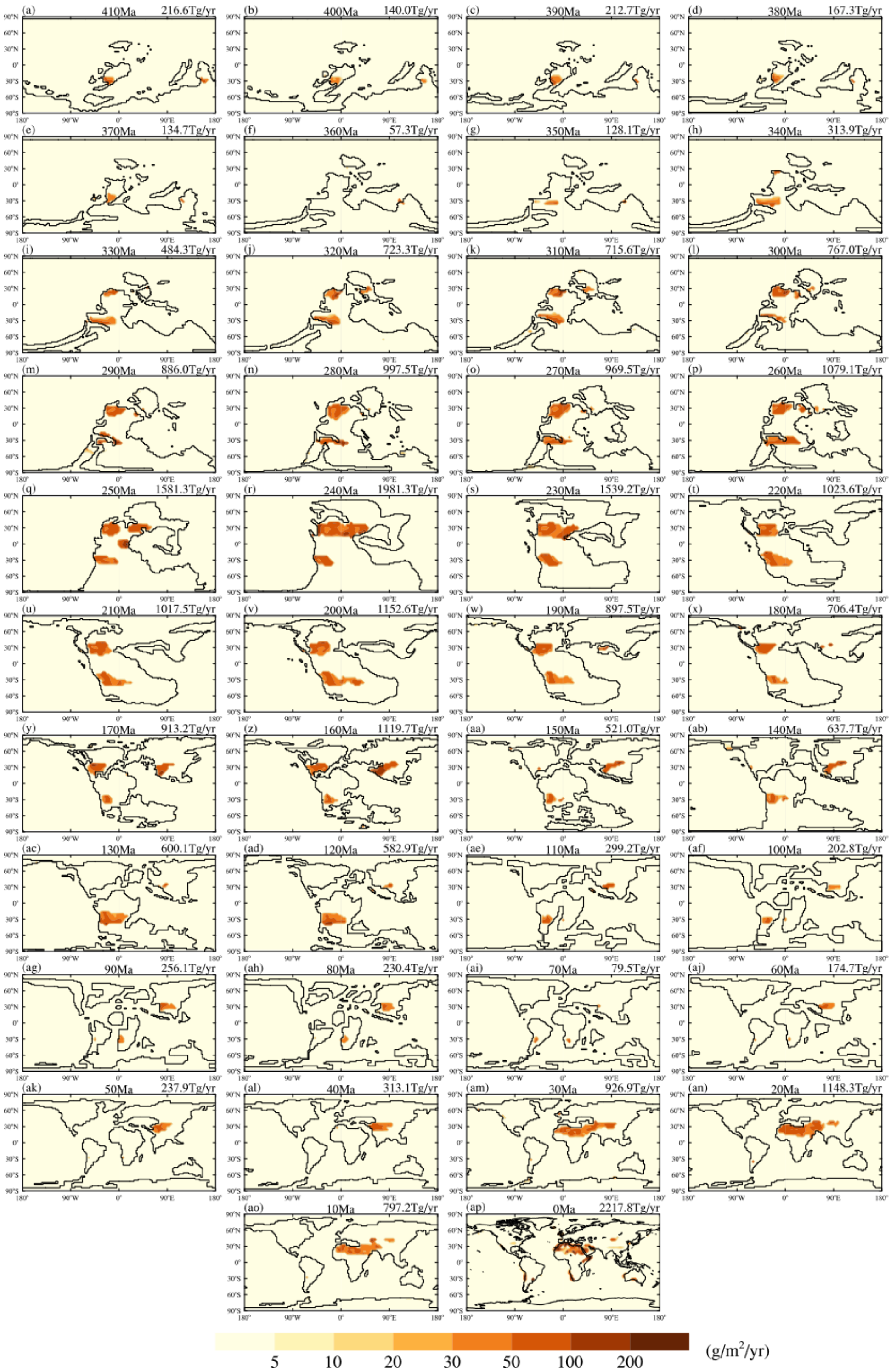

Figure 4. Annual-mean dust emission (g/m^2/yr) for 410 Ma to 0 Ma.

https://doi.org/10.5194/egusphere-2026-3925
Preprint. Discussion started: 16 July 2026

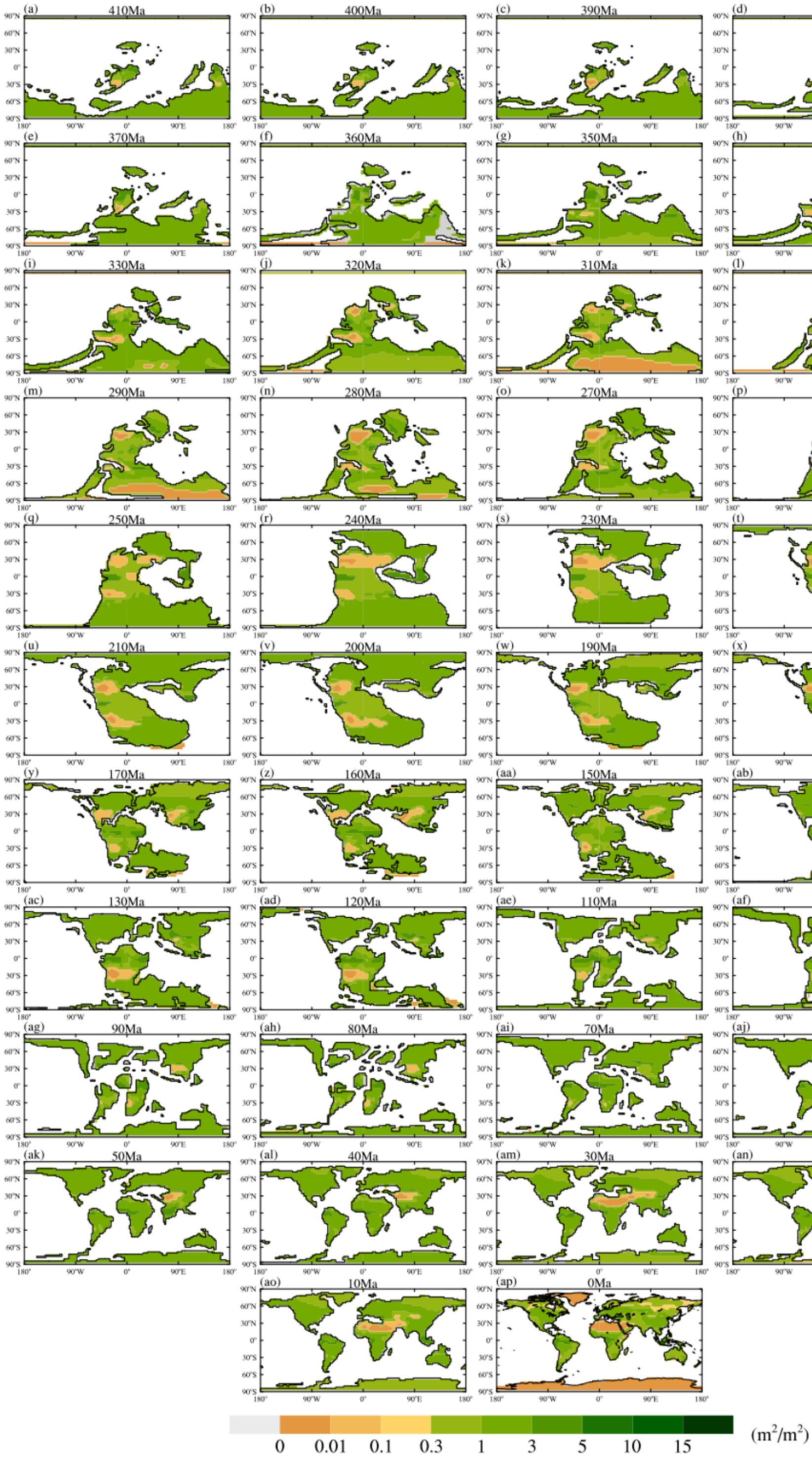

Figure 5. Vegetation cover (the sum of leaf plus stem area index) (m^2/m^2) for 410 Ma to 0 Ma.

https://doi.org/10.5194/egusphere-2026-3925
Preprint. Discussion started: 16 July 2026

3.2 Evolution of dust deposition and loading

Dust emitted to the atmosphere ultimately returns to the surface through dry or wet deposition, with the dry deposition slightly exceeding the wet deposition (Fig. 1c). Spatially, the dry deposition occurs close to where the dust is emitted (Figs. S5 and S6), while the wet deposition is much more important for the small dust particles that are transported far away from the source region (Figs. S7 and S8). As a result, over the vast area of the ocean, the deposition is mainly through wet processes, concentrated within the intertropical convergence zone (ITCZ) and mid-latitude storm track (Figs. S5-S8).

The iron content within the dust, serving as an essential nutrient, significantly influences the marine primary production and the global carbon cycle (Martin, 1990; Stoll, 2020). The trend of the total amount of dust deposited over oceans largely follows the total emission, while the fraction of dust deposited over oceans (f_{dep}_ocn) to the total deposition varies between 22% and 45%. f_{dep}_ocn is positively correlated with ocean area (Figs. 3d & 3h), which is intuitive: a larger ocean surface increases the likelihood that dust is deposited into the sea. Meanwhile, f_{dep}_ocn shows a stronger correlation with the continental fragmentation, with a correlation coefficient of 0.72 before the emergence of terrestrial vegetation (Fig. 3d) and 0.79 afterwards (Fig. 3h). Mechanistically, continental breakup reduces the distance from inland dust sources to the coast, facilitating more efficient atmospheric transport to the marine realm. From 540 Ma to 390 Ma, the fragmentation of continents generally increased with time, f_{dep}_ocn also increased, from ~37% to 45%. The continents then evolved towards a supercontinent Pangea, causing this fraction to drop to a value around 24% and remain this low during the supercontinent era (260 – 190 Ma). f_{dep}_ocn rose rapidly as Pangea broke up but dropped back sharply at 70 Ma, and remained low for the Cenozoic Era (Fig. 3h).

The simulated distributions of dust loading generally resemble those of dust deposition, with high loading occurring near major source regions and along the main transport pathways (Figs. S9–S10). Globally, total dust loading broadly tracks dust emission trends (Figs. 1b, 3c, g), confirming that emission intensity is the first-order control on atmospheric dust abundance. However, this relationship is also modulated by dust deposition. The weakened correspondence is most apparent during two paleoclimate intervals when dust loading was anomalously elevated relative to emission strengths (Fig. 1b). The first occurs during 540–520 Ma (Fig. 1b), when an anomalous reduction in global precipitation weakened wet removal and extended the atmospheric dust lifetime (Table S1). The second interval occurs during the supercontinent phase from 250 Ma to 200 Ma. The enhanced loading during this period was driven not only by strong dust emission, but also by an extended atmospheric lifetime of dust (Table S1). Two mechanisms likely contributed to this longer lifetime. First, the high GMST during the supercontinent interval may have enhanced atmospheric convection and raised the planetary boundary layer, thereby prolonging the dry lifetime of dust particles (Lin et al., 2024). Second, reduced precipitation over the supercontinent weakened wet deposition (Fig. 1c), further increasing the residence time of dust in the atmosphere.

https://doi.org/10.5194/egusphere-2026-3925
Preprint. Discussion started: 16 July 2026

3.3 Difference in Climate between DUST2 and DUST1

As previously mentioned, a globally uniform dust loading is commonly prescribed in deep-time paleoclimate simulations (Heavens et al., 2012; Kiehl & Shields, 2005; Li et al., 2022). This treatment is also used in our DUST1 experiments. In contrast, the DUST2 experiments include an active dust cycle, producing spatially heterogeneous dust loading that is dynamically linked to dust emission, transport, and deposition. The comparison between DUST1 and DUST2, therefore, provides a useful test of how the assumption of globally uniform dust loading affects simulated land surface climate.

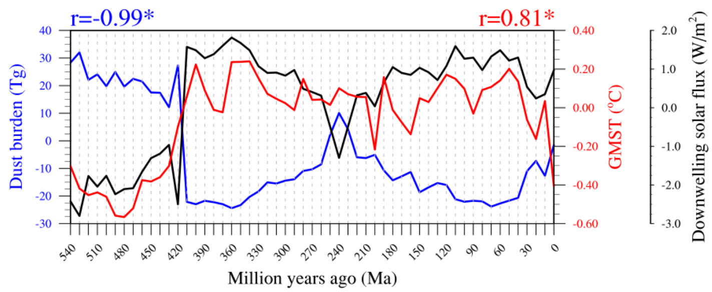

Figure 6. The difference in GMST (°C), dust burden (Tg), and surface downwelling solar flux (W/m^2) between DUST2 experiments and DUST1 experiments (DUST2 – DUST1). The upper right and left corners display the correlation coefficients between surface downwelling solar flux and GMST, and between surface downwelling solar flux and dust burden. (*) indicates statistical significance at the 95% confidence level.

Dust affects the climate mainly through its radiative effects. Airborne dust scatters and absorbs radiation, reducing the shortwave radiation reaching the surface while heating the atmosphere; under cold climates with high dust loading, this atmospheric heating may even contribute to surface warming (Liu et al., 2021). Dust deposited on snow and ice can also darken the surface and reduce albedo, producing an additional warming effect (Shi et al., 2019a; Xie et al., 2018). Dust may further influence clouds and precipitation through indirect effects, but these indirect effects are not represented in the CAM4 dust scheme used here. Therefore, our analysis focuses on the direct radiative effect of atmospheric dust and the snow-darkening effect of deposited dust, with particular attention to shortwave radiation because it dominates the dust-induced surface energy changes in our simulations. Compared to DUST1 experiments, the global dust loading is generally lower in DUST2 experiments except during the periods before plant colonization (540 – 420 Ma) and the supercontinent era (~250 Ma; blue curve in Fig. 6). Consistent with this difference in dust loading, the global mean surface temperature (GMST) is generally slightly higher in DUST2 than in DUST1 from 410 Ma to 10 Ma, with differences mostly smaller than 0.25 °C. In contrast, during 540–420 Ma, when DUST2 has substantially higher dust loading than DUST1, GMST is lower by approximately 0.3–0.5 °C (red curve in Fig. 6). This global-scale relationship suggests that the imposed uniform dust loading in DUST1 may underestimate the cooling effect of dust during vegetation-free intervals, but may overestimate it during much of the post-plant-colonization interval.

https://doi.org/10.5194/egusphere-2026-3925
Preprint. Discussion started: 16 July 2026

The spatial pattern of temperature change further supports this interpretation. In regions where DUST2 dust loading exceeds that in DUST1 (Figs. S11 and S12), land surface cooling is commonly observed (Figs. 7 and 8), with maximum cooling reaching about 4.0 °C before plant colonization and about 1.5 °C afterwards. These cooling regions generally coincide with major dust source regions and high dust loading areas. This local cooling is induced by the reduction of the shortwave radiation reaching the surface (Figs. S13-S14). To isolate the dust's direct impact from cloud-related interference, we additionally examined the clear-sky downwelling shortwave radiation (Figs. S15-S16), which confirms the primary role of dust in surface cooling. Nevertheless, the total surface temperature response is not determined by radiation alone. In several regions, especially during 540–420 Ma, increased snow cover amplifies the initial cooling through a positive snow–albedo feedback (Figs. S17). Note that the snow-darkening effect of dust is considered in the model we use, but it is too weak to stop snow from expanding in most cases. Therefore, the local cooling in DUST2 reflects a combination of dust-induced shortwave reduction and subsequent surface-albedo feedbacks. A different response occurs in the equatorial regions during 540–420 Ma. Although dust loading in DUST2 is higher than in DUST1 (Fig. S11), these regions warm by up to 3.45 °C (Fig. 7). This warming is accompanied by a substantial decrease in cloud cover (Fig. S19) and an associated increase in shortwave cloud forcing (Fig. S20). In this case, the increase in solar radiation associated with reduced cloud reflection appears to outweigh the dust-induced reduction in clear-sky shortwave radiation, leading to net surface warming.

For regions where dust loading is lower in DUST2 than in DUST1, which mainly occurs during 410–10 Ma (Figs. S12), land surface temperature is generally higher (Fig. 8). This warming is consistent with weaker dust attenuation of incoming shortwave radiation (Figs. S14). In many regions, the warming might be further reinforced by reduced snow cover and lower surface albedo (Fig. S18). However, several exceptions indicate that the climate response is strongly modulated by multiple feedbacks. During 320 Ma, 170 Ma, and 160 Ma, mid- to high-latitude cooling occurs even though DUST2 dust loading is lower than in DUST1. Under these relatively cold background climates, reduced dust deposition on snow may weaken the snow-darkening effect, thereby increasing snow albedo and favoring local cooling. Clouds can also play an important role; it enhances the southern polar cooling at 200 Ma while the northern polar cooling during 170-160 Ma and 30–10 Ma (Figs S21-S22). These results suggest that cloud shading, together with the snow–albedo feedback, offsets, or even reverses, the warming expected from lower dust loading.

Overall, the DUST1–DUST2 comparison shows that the assumption of globally uniform dust loading can affect simulated surface climate in a spatially and temporally heterogeneous way. The first-order response of either local or global surface temperature is broadly consistent with differences in dust loading and shortwave radiative attenuation. However, the eventual surface temperature response also depends strongly on cloud changes, snow cover, and associated surface-albedo feedbacks. Therefore, interactive dust simulations are necessary not only for representing the spatial distribution of dust loading, but also for capturing the coupled dust–climate feedbacks that cannot be represented by a globally uniform dust prescription.

https://doi.org/10.5194/egusphere-2026-3925
Preprint. Discussion started: 16 July 2026

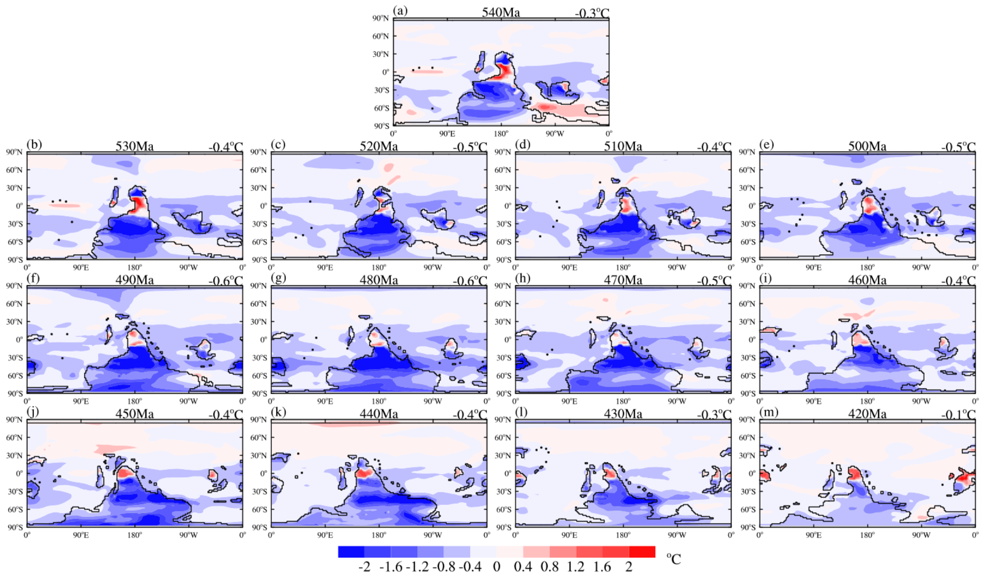

Figure 7. The differences in surface temperature (°C) between DUST2 experiments and DUST1 experiments for 540 Ma-420Ma.

https://doi.org/10.5194/egusphere-2026-3925
Preprint. Discussion started: 16 July 2026

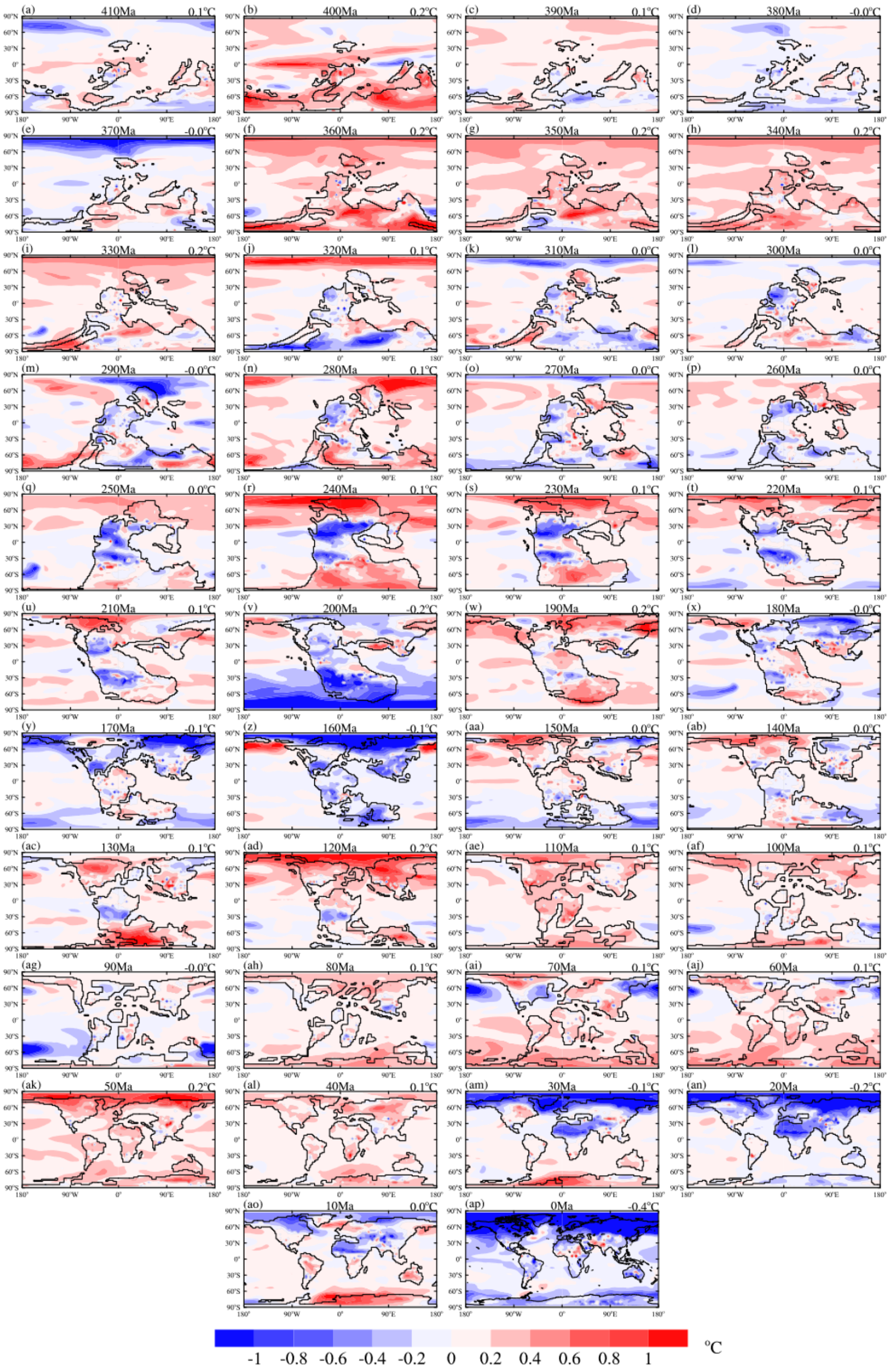

Figure 8. The differences in surface temperature (°C) between DUST2 experiments and DUST1 experiments for 410 Ma to 0 Ma.

https://doi.org/10.5194/egusphere-2026-3925
Preprint. Discussion started: 16 July 2026

4. Model-Records Comparison

The simulated dust deposition (Figs. 9-10) enables direct comparison with records of aeolian sand systems. In order to do this comparison, we searched all the literature that presented evidence of ancient loess deposits, subaquatic dust deposits, aeolian sand systems, and their preserved successions (a full list can be found in Table S2). We focus on the periods after plant colonization; the model results cannot be tested effectively with sparse records before plant colonization since dust was likely deposited everywhere. The sites of the records we found are shown as blue pentagrams in Fig. 10. Because most of the records were given only a vague date, very often only specific to a certain Era, we treat them as indicating the presence of dust deposition over the whole period. For example, the same records are used for the three time slices between 410 – 390 Ma and those between 360 – 330 Ma, respectively. Other than 380 – 370 Ma, 290 – 270 Ma, 220 – 210 Ma, 60 Ma, and 30 – 20 Ma, dust records are available for all (32 out of 42) the time slices (Figs. 9-10).

It can be seen from Fig. 10 that the simulated dust deposition is, in general, compatible with the distribution of record sites, but the model severely underestimates the dust production and deposition in certain periods. At 360 Ma, model simulation produces almost no dust (Fig. 9f) due to extensive vegetation cover (Fig. 10f), contrasting with the existence of dust records at three sites. It is noticeable that the model-proxy discrepancy becomes more severe since the beginning of the formation of the Atlantic Ocean (from 100 Ma; Fig. 9). The reason for such model-proxy discrepancy is unclear; it could be due to either the uncertainties in the reconstruction of paleogeography or the biases in vegetation modeling and warrants further investigations in the future.

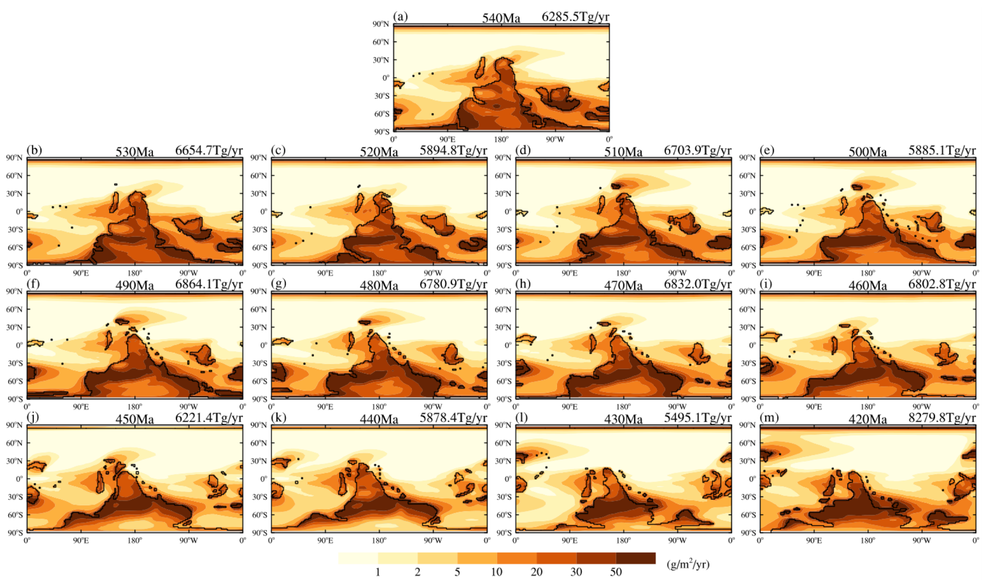

Figure 9. Annual-mean dust deposition (g/m^2/yr) for 540 Ma-420Ma.

https://doi.org/10.5194/egusphere-2026-3925
Preprint. Discussion started: 16 July 2026

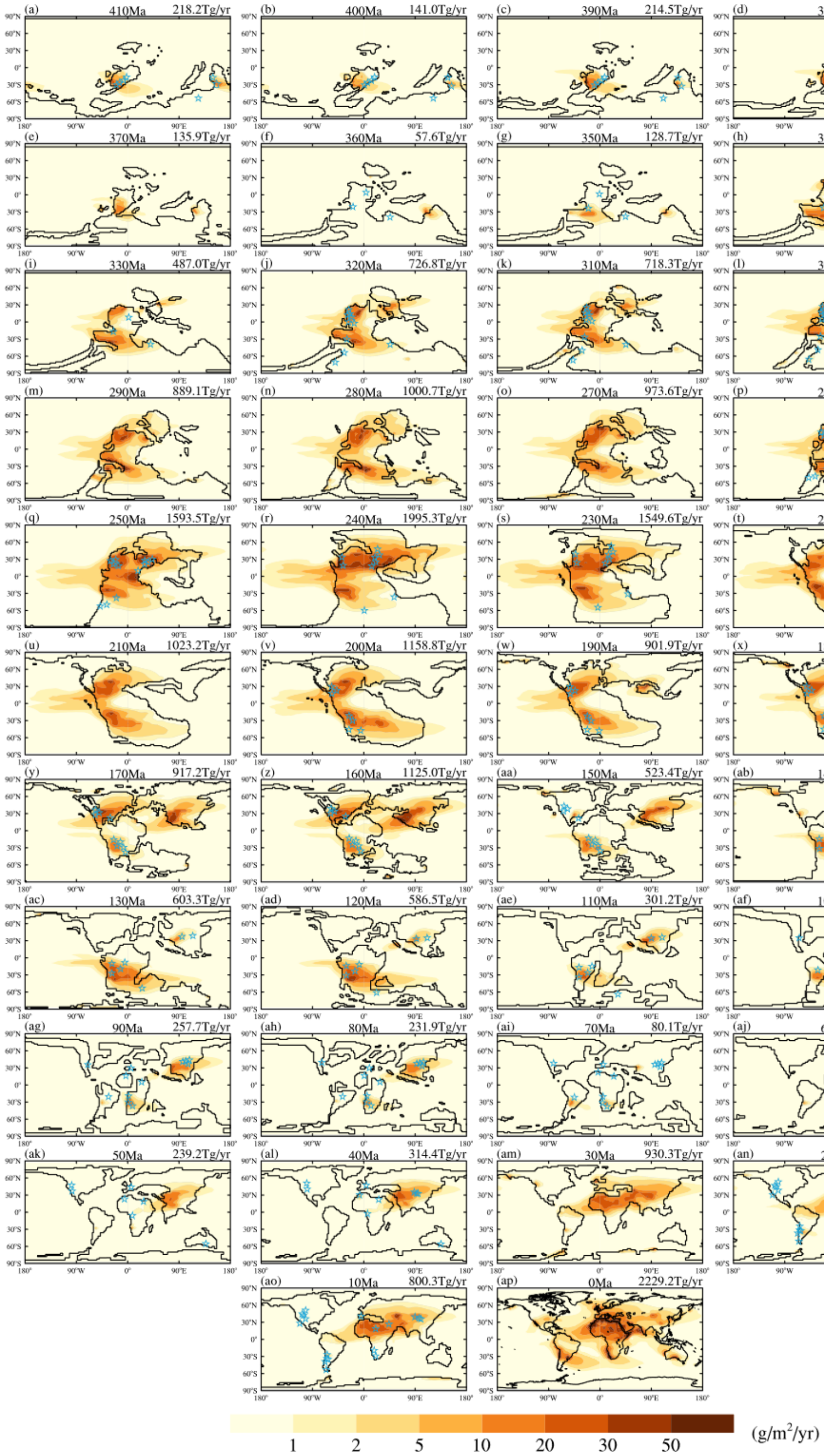

Figure 10. Annual-mean dust deposition (g/m^2/yr) for 410 Ma to 0 Ma. Blue pentagrams indicate the locations of records of aeolian sand systems (full list and references in Table S2).

https://doi.org/10.5194/egusphere-2026-3925
Preprint. Discussion started: 16 July 2026

5. Discussion

Although the simulated geographic distribution of dust deposition compares well with the available records in general, there are obvious discrepancies. For example, the simulations substantially underestimate the extent of dust since 100 Ma (Fig. 10). Such a discrepancy could be due to the uncertainties in our model, especially in vegetation simulation. Other than that, the climatic impact of dust presented above also suffers from deficiencies in the model and experimental design. These uncertainties and deficiencies are described in detail below.

5.1 Uncertainties due to Soil Erodibility

Lin et al. (2024) discussed the uncertainties introduced by using a globally uniform soil erodibility k and BIOME4 vegetation model in simulations, highlighting issues such as the underestimation of dust emission over hotspot regions and the overestimation of dust in subtropical regions. These issues should also be present in this study, which leads to the discrepancies between local observational results and simulation outputs. Moreover, using a globally uniform *k* leads to an overestimation of dust emissions in coastal regions, resulting in greater dust deposition over the ocean (Lin et al., 2024). In this study, the simulated proportion of dust deposited into the ocean at 0 Ma reached as high as 44.5% (Fig. 3f), significantly higher than the results based on more realistic *k* distributions: 16% and 26% (Albani et al., 2016; Jickells et al., 2005). We believe that this overestimation likely persists across all experiments in this study. However, the relative magnitudes of dust emissions and deposition across different periods remain reasonably credible.

5.2 Uncertainty in Vegetation Distribution

The uncertainty in vegetation simulation affects the dust cycle mainly through the distribution of dust source regions. The vegetation model used herein, BIOME4, is unable to reproduce the present-day vegetation distribution as demonstrated in Lin et al. (2024). This is a common problem with all vegetation models (Dallmeyer et al., 2026; Kaplan et al., 2003a; Lunt et al., 2012; Zhang et al., 2015; Zhao et al., 2025), and the problem may not be solely attributed to the deficiency in the vegetation model but also that in the climate model. How well such coupled climate-vegetation models perform in the deep past is even uncertain and can only be constrained by paleo records, which are sparse.

Moreover, terrestrial vegetation has undergone a complex evolutionary process over the past 540 million years. In this study, we set the emergence of angiosperms at 100 Ma. Compared to gymnosperms, angiosperms exhibit more efficient photosynthesis and higher transpiration rates (Boyce et al., 2009) and may be better adapted to arid conditions. We set the emergence of C4 plants at 10 Ma. Compared to C3 plants, C4 vegetation has a more complex and efficient photosynthetic mechanism, enabling it to sustain photosynthesis even when stomata are closed. This adaptation makes C4 plants better suited to harsh climatic conditions, such as high temperatures and drought (Edwards et al., 2010; Sage & Pearcy, 2000). Detailed tests by Lin et al. (2024) have shown that invoking or not invoking C4 and angiosperms had a minor influence on the simulated dust emission and loading. Therefore, when to let angiosperms and C4 appear should not have a large influence on the results obtained herein. However, plant evolution is a complex process, involving morphological structures, physiological functions, climatic thresholds, and other factors (Sun et al., 2012), especially during the early periods when plants just landed (Dahl & Arens, 2020). The simplified settings used in this study are insufficient to thoroughly investigate the impacts of vegetation evolution on the dust cycle. Future research, with improved vegetation models, will thus be essential to better represent early vegetation and simulate the dust cycle.

5.3 Uncertainties in Dust's Climatic Effect

There are several uncertainties and limitations in our understanding of the dust climate effect. First, the transient nature of the DUST2 experiments limits their ability to capture long-term climate feedbacks. Because the DUST2 simulations were integrated for only 100 model years, they predominantly reflect the relatively rapid responses of the atmosphere, land surface, sea ice, and upper ocean mixed layer. Consequently, they cannot fully represent the sluggish adjustment of the deep ocean and the comprehensive reorganization of large-scale ocean circulation.

Second, our simulations do not account for the indirect radiative effects of dust. While the direct effect of dust on longwave and shortwave radiation is resolved, its indirect effects—primarily mediated through dust particles acting as cloud condensation nuclei (CCN) or ice nucleating particles (INPs)—are significant but remain beyond the scope of the current model configuration (Kok et al., 2023). Dust-cloud interactions can dramatically alter cloud albedo, lifetime, and precipitation patterns, which subsequently influence regional hydrological cycles and temperature fields. The absence of these indirect radiative pathways means that the total climate feedback induced by the dust cycle might be either amplified or dampened in certain regions.

Third, the simplified configurations of dust particle size distribution and complex refractive index introduce additional uncertainties. The direct radiative forcing of airborne mineral dust is highly sensitive to its microphysical and optical properties (Wang et al., 2024). In our dust module, the representation of particle size bins and the complex refractive index is idealized and globally uniform. This simplification limits the model's capacity to capture the full spectral and regional variations of dust radiative properties. In reality, dust from different paleo-source regions would exhibit distinct mineralogical compositions and coarseness, which could significantly alter the local ratio of solar absorption to scattering. Future paleoclimate simulations would highly benefit from incorporating more sophisticated, heterogeneous microphysical parameterizations.

6. Summary

This study provides a Phanerozoic-scale simulation of global dust activity and its climatic impacts by coupling an Earth system model, CESM1.2.2, and a vegetation model, BIOME4. The results show that the colonization of land by plants near the end of the Silurian caused a fundamental reorganization of the global dust cycle. Before plant colonization (set to be before 410

https://doi.org/10.5194/egusphere-2026-3925
Preprint. Discussion started: 16 July 2026

Ma herein), dust emission could occur over nearly all snow-free terrestrial surfaces but preferentially from subtropical regions where soil is dry and coastal regions where wind is strong. During this interval (540 Ma-420 Ma), the global dust emission varied between 5,400 and 8,200 Tg/yr (1.5×10^{-9}-2.4×10^{-9} kg/m^2/s), and the atmospheric dust loading varied between 37 and 57 Tg/yr, much higher than those for 0 Ma (2,218 Tg/yr and 23.4 Tg/yr, respectively). This emission is an order of magnitude higher than that obtained by Xie et al. (2024), where they estimated a range of 0.4×10^{-10}-2.1×10^{-10} kg/m^2/s. A robust relation could not be found between global dust emission and continental configuration (global or subtropical continental area or fragmentation), unlike for the interval after the plant colonization (410 Ma – 0 Ma). The climate has some impact on the dust emission, with the snow cover strongly prohibiting dust emission during cold climate periods. However, there is no clear relation between global dust emission and GMST. Dust activity during this interval was therefore controlled mainly by the spatial overlap among dry land, strong surface winds, and snow cover.

After plant colonization, vegetation shielding sharply reduced the extent of erodible land, causing a large decline in dust source area, dust emission, and atmospheric dust loading. In contrast to the previous interval, the global dust emission and dust loading in this interval could vary by one and a half orders of magnitude; they change from 57 to 2,218 Tg/yr and 0.5 to 35 Tg/yr, respectively. During this interval, dust sources became largely restricted to unvegetated or sparsely vegetated subtropical regions. Thus, subtropical land area and continental fragmentation have acted as key controls on dust emission during 410 Ma – 0 Ma (Fig. 3), by regulating the availability of dry, vegetation-poor dust source regions. The largest emission appeared at 250 Ma, at which the subtropical land area was among the highest, while the continental fragmentation was the lowest, and the lowest emission appeared at 70 Ma, when the subtropical land area was the smallest and continents were most fragmented.

A major consequence of the changing dust cycle is the long-term variation in dust deposition to the ocean. Although total ocean dust deposition broadly follows global dust emission, the fraction of dust deposited over the ocean is strongly regulated by continental configuration. More fragmented continents allow dust to be transported more efficiently to the ocean, whereas supercontinent configurations reduce the oceanic fraction of dust deposition. Because dust supplies iron and other nutrients to marine ecosystems, these changes in ocean dust deposition may have influenced marine productivity and the global carbon cycle through geological time.

The simulations also show that dust can exert substantial climatic effects. Compared with experiments using globally uniform prescribed dust loading (DUST1), the interactive dust-cycle experiments (DUST2) produce spatially heterogeneous dust loading and therefore more realistic regional radiative forcing. Dust generally cools the local surface by reducing incoming shortwave radiation, but the final temperature response is strongly modulated by snow–albedo feedbacks, cloud changes, sea ice, and possibly ocean circulation. Unsurprisingly, GMST is 0.3-0.5 °C lower in DUST2 than in DUST1 during 540 Ma – 420 Ma, because the dust loading was substantially underestimated in the latter. The GMST change between DUST2 and DUST1 is generally small (<0.2 °C) during 410 Ma – 0 Ma, but local temperature changes can be as large as ±1.5 °C. The comparison between DUST2 and DUST1 shows that less dust may not result in a warmer climate. For example, there is less dust in DUST2 than in DUST1 for many of the time slices (e.g. 200 Ma, 160 Ma, 30, and 20 Ma), but GMST is actually lower in DUST2 (Fig. 6). Such cooling could be due to weaker snow-darkening effect when there is less dust, but further study is warranted to fully understand the underlying mechanisms, for instance, the ocean circulation. Note that since the simulations in DUST2 were carried out for only 100 years, the climatic impact of dust obtained herein represents only the fast response of the climate system. Although Lin et al. (2024) have shown that long-term climate response to dust remains small under warm background climate, it could be much larger (>2 °C) under cold climate, as demonstrated for the LGM (Zhang et al., 2022).

Our study also reveals a significant problem in the model simulations; there seems to be a systematic low bias in the simulated dust amount since 100 Ma compared to geological records (Fig. 10). It is unclear what could cause such a model-data discrepancy. Model deficiency certainly cannot be ruled out, but it is also possible that the records were preserved under different orbital configurations. If the bias does not affect the dust amount too much, then the present-day dust emission and atmospheric dust loading may be the highest over the past 200 Ma, comparable to those in the Pangea supercontinent era (Fig. 3). This high dust emission is mainly due to the large subtropical land area in the present day.

Overall, the results show that long-term changes in terrestrial vegetation, continental configuration, and climate jointly regulated dust source activity, atmospheric loading, deposition to the ocean, and climatic effects, making dust an evolving and spatially heterogeneous component of the Earth system rather than a passive indicator of aridity. Future work integrating improved geological constraints and more realistic dust–vegetation–climate interactions will be important for better evaluating the role of dust in Phanerozoic environmental change.

Code and data availability.

The source code of CESM1.2.2 can be accessed at https://www.cesm.ucar.edu/models/cesm1.2.

Author contributions

The study was developed by all authors. Y.L. and Y.H. conceived the study and contributed to the writing. Q.L. and J.G. set up the model and designed the experiments. Q.C. performed the analyses, prepared the figures, and wrote the initial manuscript. Q.L., Y. L., X. B., X. L., Z. L., S. Y., Y. C., and S. Z. contributed to the model simulations. J. Z. and H. Z. provided guidance on the analysis.

Competing interests

The contact author has declared that none of the authors have any competing interests.

Acknowledgments

Simulations were conducted at the High-performance Computing Platform of Peking University. We would like to thank Jiawenjing Lan, Zhihong Song, Zihan Yin, and Mengyu Wei for their helpful assistance with the numerical simulations.

Financial support

This work is supported by the National Natural Science Foundation of China (grant No. 42488201 and 42225606)

References

Albani, S., N. M. Mahowald, A. T. Perry, R. A. Scanza, C. S. Zender, N. G. Heavens, et al. Improved dust representation in the Community Atmosphere Model. Journal of Advances in Modeling Earth Systems (2014).

Albani, S., N. M. Mahowald, G. Winckler, R. F. Anderson, L. I. Bradtmiller, B. Delmonte, et al. Twelve thousand years of dust: the Holocene global dust cycle constrained by natural archives. Climate of the Past 11(6), 869-903 (2015). https://doi.org/10.5194/cp-11-869-2015

Albani, S., N. M. Mahowald, L. N. Murphy, R. Raiswell, J. K. Moore, R. F. Anderson, et al. Paleodust variability since the Last Glacial Maximum and implications for iron inputs to the ocean. Geophysical Research Letters 43(8), 3944-3954 (2016). https://doi.org/10.1002/2016GL067911

Andreae, M. O. & D. Rosenfeld. Aerosol-cloud-precipitation interactions. Part 1. The nature and sources of cloud-active aerosols. Earth-Science Review 89(1-2), 13-41 (2008). https://doi.org/10.1016/j.earscirev.2008.03.001

Atkinson, J. D., B. J. Murray, M. T. Woodhouse, T. F. Whale, K. J. Baustian, K. S. Carslaw, et al. The importance of feldspar for ice nucleation by mineral dust in mixed-phase clouds. Nature 498(7454), 355-358 (2013). https://doi.org/10.1038/nature12278

Boyce, C. & J. E. Lee. Plant Evolution and Climate Over Geological Timescales. (2017).

Boyce, C. K., T. J. Brodribb, T. S. Feild & M. A. Zwieniecki. Angiosperm leaf vein evolution was physiologically and environmentally transformative. Proceedings of the Royal Society B: Biological Sciences 276(1663), 1771-1776 (2009). https://doi.org/10.1098/rspb.2008.1919

Castillo, C. K. G., S. Levis & P. Thornton. Evaluation of the New CNDV Option of the Community Land Model: Effects of Dynamic Vegetation and Interactive Nitrogen on CLM4 Means and Variability. Journal of Climate 25(11), 3702-3714 (2012). https://doi.org/10.1175/JCLI-D-11-00372.1

Cerling, T. E., J. M. Harris, B. J. MacFadden, M. G. Leakey, J. Quade, V. Eisenmann & J. R. Ehleringer. Global vegetation change through the Miocene/Pliocene boundary. Nature 389(6647), 153-158 (1997). https://doi.org/10.1038/38229

Cosentino, N. J., G. Torre, F. Lambert, S. Albani, F. De Vleeschouwer & A. J. M. Bory. Paleo±Dust: quantifying uncertainty in paleo-dust deposition across archive types. Earth Syst. Sci. Data 16(2), 941-959 (2024). https://doi.org/10.5194/essd-16-941-2024

Dahl, T. W. & S. K. M. Arens. The impacts of land plant evolution on Earth's climate and oxygenation state – An interdisciplinary review. Chemical Geology 547, 119665 (2020). https://doi.org/https://doi.org/10.1016/j.chemgeo.2020.119665

Dallmeyer, A., N. Weitzel, L. Schild, U. Herzschuh, T. Kleinen & M. Claussen. Unravelling the tree cover dynamics over the last 20 000 years on the Northern Hemisphere. Clim. Past 22(6), 1125-1157 (2026). https://doi.org/10.5194/cp-22-1125-2026

Edwards, E. J., C. P. Osborne, C. A. E. Strömberg, S. A. Smith, C. G. Consortium, W. J. Bond, et al. The Origins of C4 Grasslands: Integrating Evolutionary and Ecosystem Science. Science 328(5978), 587-591 (2010). https://doi.org/10.1126/science.1177216

Gough, D. O. Solar interior structure and luminosity variations. Solar Physics 74(1), 21-34 (1981). https://doi.org/10.1007/BF00151270

Guo, Z. T., S. Z. Peng, Q. Z. Hao, P. E. Biscaye & T. S. Liu. Origin of the Miocene-Pliocene Red-Earth formation at Xifeng in northern China and implications for paleoenvironments. Palaeogeography Palaeoclimatology Palaeoecology 170(1-2), 11-26 (2001). https://doi.org/10.1016/S0031-0182(01)00235-8

Heavens, N. G., C. A. Shields & N. M. Mahowald. A paleogeographic approach to aerosol prescription in simulations of deep time climate. Journal of Advances in Modeling Earth Systems 4(4) (2012). https://doi.org/https://doi.org/10.1029/2012MS000166

Hu, Y., X. Li, W. R. Boos, J. Guo, J. Lan, Q. Lin, et al. Emergence of the modern global monsoon from the Pangaea megamonsoon set by palaeogeography. Nature Geoscience 16(11), 1041-1046 (2023). https://doi.org/10.1038/s41561-023-01288-y

Huang, J. P., T. H. Wang, W. C. Wang, Z. Q. Li & H. R. Yan. Climate effects of dust aerosols over East Asian arid and semiarid regions. Journal of Geophysical Research-Atmospheres 119(19), 11398-11416 (2014). https://doi.org/10.1002/2014JD021796

Hurrell, J. W., M. M. Holland, P. R. Gent, S. Ghan, J. E. Kay, P. J. Kushner, et al. The Community Earth System Model: A Framework for Collaborative Research. Bulletin of the American Meteorological Society 94(9), 1339-1360 (2013). https://doi.org/10.1175/bams-d-12-00121.1

Jickells, T. D., Z. S. An, K. K. Andersen, A. R. Baker, G. Bergametti, N. Brooks, et al. Global Iron Connections Between Desert Dust, Ocean Biogeochemistry, and Climate. Science 308(5718), 67-71 (2005). https://doi.org/10.1126/science.1105959

Kaplan, J. O., N. H. Bigelow, I. Prentice, S. Harrison, P. J. Bartlein, T. R. Christensen, et al. Climate change and Arctic ecosystems: 2. Modeling, paleodata-model comparisons, and future projections. Journal of Geophysical Research D: Atmospheres 108(19) (2003a). https://doi.org/10.1029/2002jd002559

Kaplan, J. O., N. H. Bigelow, I. C. Prentice, S. P. Harrison, P. J. Bartlein, T. R. Christensen, et al. Climate change and Arctic ecosystems: 2. Modeling, paleodata-model comparisons, and future projections - art. no. 8171. Journal of Geophysical Research-Atmospheres 108(D19) (2003b). https://doi.org/10.1029/2002JD002559

Kiehl, J. T. & C. A. Shields. Climate simulation of the latest Permian: Implications for mass extinction. Geology 33(9), 757-760 (2005). https://doi.org/10.1130/G21654.1

Kok, J. F., T. Storelvmo, V. A. Karydis, A. A. Adebiyi, N. M. Mahowald, A. T. Evan, et al. Mineral dust aerosol impacts on global climate and climate change. Nature Reviews Earth & Environment 4(2), 71-86 (2023). https://doi.org/10.1038/s43017-022-00379-5

Krinner, G., O. Boucher & Y. Balkanski. Ice-free glacial northern Asia due to dust deposition on snow. Climate Dynamics 27(6), 613-625 (2006). https://doi.org/10.1007/s00382-006-0159-z

Kushta, J., G. Kallos, M. Astitha, S. Solomos, C. Spyrou, C. Mitsakou & J. Lelieveld. Impact of natural aerosols on atmospheric radiation and consequent feedbacks with the meteorological and photochemical state of the atmosphere. Journal of Geophysical Research-Atmospheres 119(3), 1463-1491 (2014). https://doi.org/10.1002/2013JD020714

Li, H.-T., T.-S. Yi, L.-M. Gao, P.-F. Ma, T. Zhang, J.-B. Yang, et al. Origin of angiosperms and the puzzle of the Jurassic gap. Nature Plants (2019).

Li, X., Y. Hu, J. Guo, J. Lan, Q. Lin, X. Bao, et al. A high-resolution climate simulation dataset for the past 540 million years. Scientific Data (2022).

Lin, Q., Y. Liu, J. Guo, X. Li, J. Lan, H. Zuo, et al. Simulated dust activity in typical time periods of the past 250 million years. Fundamental Research 6(2), 963-973 (2024). https://doi.org/10.1016/j.fmre.2024.02.004

Liu, P., Y. Liu, Y. Peng, J.-F. Lamarque, M. Wang & Y. Hu. Large influence of dust on the Precambrian climate. Nature Communications 11(1), 4427 (2020). https://doi.org/10.1038/s41467-020-18258-2

Liu, Y. G., P. Liu, D. W. Li, Y. R. Peng & Y. Y. Hu. Influence of Dust on the Initiation of Neoproterozoic Snowball Earth Events. Journal of Climate 34(16), 6673-6689 (2021). https://doi.org/10.1175/JCLI-D-20-0803.1

Lunt, D. J., T. Dunkley Jones, M. Heinemann, M. Huber, A. LeGrande, A. Winguth, et al. A model–data comparison for a multi-model ensemble of early Eocene atmosphere–ocean simulations: EoMIP. Clim. Past 8(5), 1717-1736 (2012). https://doi.org/10.5194/cp-8-1717-2012

Maher, B. A., J. M. Prospero, D. Mackie, D. Gaiero, P. P. Hesse & Y. Balkanski. Global connections between aeolian dust, climate and ocean biogeochemistry at the present day and at the last glacial maximum. Earth-Science Reviews 99(1), 61-97 (2010). https://doi.org/https://doi.org/10.1016/j.earscirev.2009.12.001

Martin, J. H. Glacial-Interglacial CO2 Change: The Iron Hypothesis. Paleoceanography 5(1), 1-13 (1990). https://doi.org/10.1029/PA005i001p00001

Miller, R. L. & I. Tegen. Climate response to soil dust aerosols. Journal of Climate 11(12), 3247-3267 (1998). https://doi.org/10.1175/1520-0442(1998)011<3247:CRTSDA>2.0.CO;2

Miller, R. L., P. Knippertz, C. P. García-Pando, J. P. Perlwitz & I. Tegen (2014). Impact of Dust Radiative Forcing upon Climate.

Neale, R., J. Richter, A. Conley, S. Park, P. Lauritzen, A. Gettelman, et al. Description of the Community Atmosphere Model (CAM 4.0). NCAR Technical Note TN-485+STR (2010).

Okin, G. S., N. Mahowald, O. A. Chadwick & P. Artaxo. Impact of desert dust on the biogeochemistry of phosphorus in terrestrial ecosystems. Global Biogeochemical Cycles 18(2) (2004). https://doi.org/https://doi.org/10.1029/2003GB002145

Sage, R. F. & R. W. Pearcy. The Physiological Ecology of C4 Photosynthesis.In R. C. Leegood, T. D. Sharkey and S. von Caemmerer. Photosynthesis: Physiology and Metabolism: 497-532. Dordrecht, Springer Netherlands (2000).

Sakaeda, N., R. Wood & P. J. Rasch. Direct and semidirect aerosol effects of southern African biomass burning aerosol. Journal of Geophysical Research-Atmospheres 116 (2011). https://doi.org/10.1029/2010JD015540

Salles, T., L. Husson, M. Lorcery & B. Hadler Boggiani. Landscape dynamics and the Phanerozoic diversification of the biosphere. Nature 624(7990), 115-121 (2023). https://doi.org/10.1038/s41586-023-06777-z

Scotese, C. Phanerozoic Global Temperature Curve (2016).

Scotese, C. R., H. J. Song, B. J. W. Mills & D. G. van der Meer. Phanerozoic paleotemperatures: The earth's changing climate during the last 540 million years. Earth-Science Reviews 215 (2021). https://doi.org/10.1016/j.earscirev.2021.103503

Scotese, R. S. & N. Wright. PALEOMAP Paleodigital Elevation Models (PaleoDEMS) for the Phanerozoic. https://www.earthbyte.org/paleodem-resource-scotese-and-wright-2018/ (2018).

Shi, Z., X. Liu, Z. An, B. Yi, P. Yang & N. Mahowald. Simulated variations of eolian dust from inner Asian deserts at the mid-Pliocene, last glacial maximum, and present day: contributions from the regional tectonic uplift and global climate change. Climate Dynamics 37(11), 2289-2301 (2011). https://doi.org/10.1007/s00382-011-1078-1

Shi, Z., X. Xie, X. Li, L. Yang, X. Xie, J. Lei, et al. Snow-darkening versus direct radiative effects of mineral dust aerosol on the Indian summer monsoon onset: role of temperature change over dust sources. Atmospheric Chemistry and Physics 19(3), 1605-1622 (2019a).

Shi, Z. G., X. N. Xie, X. Z. Li, L. Yang, X. X. Xie, J. Lei, et al. Snow-darkening versus direct radiative effects of mineral dust aerosol on the Indian summer monsoon onset: role of temperature change over dust sources. Atmospheric Chemistry and Physics 19(3), 1605-1622 (2019b). https://doi.org/10.5194/acp-19-1605-2019

Soreghan, G. S., N. G. Heavens, L. A. Hinnov, S. M. Aciego & C. Simpson. Reconstructing the Dust Cycle in Deep Time: the Case of the Late Paleozoic Icehouse. The Paleontological Society Papers 21, 83-120 (2015). https://doi.org/10.1017/s1089332600002977

Stoll, H. 30 years of the iron hypothesis of ice ages. Nature 578(7795), 370 (2020). https://doi.org/10.1038/d41586-020-00393-x

Sun, Y. D., M. M. Joachimski, P. B. Wignall, C. B. Yan, Y. L. Chen, H. S. Jiang, et al. Lethally Hot Temperatures During the Early Triassic Greenhouse. Science 338(6105), 366-370 (2012). https://doi.org/10.1126/science.1224126

Wang, H., X. Liu, C. Wu, G. Lin, T. Dai, D. Goto, et al. Larger Dust Cooling Effect Estimated From Regionally Dependent Refractive Indices. Geophysical Research Letters 51(9), e2023GL107647 (2024). https://doi.org/https://doi.org/10.1029/2023GL107647

Xie, X., X. Liu, H. Che, X. Xie, X. Li, Z. Shi, et al. Radiative feedbacks of dust in snow over eastern Asia in CAM4-BAM. Atmos. Chem. Phys. 18(17), 12683-12698 (2018). https://doi.org/10.5194/acp-18-12683-2018

Xie, Y., D. J. Lunt & P. J. Valdes. Diagnosing the controls on desert dust emissions through the Phanerozoic. Climate of the Past 20(11), 2561-2585 (2024). https://doi.org/10.5194/cp-20-2561-2024

Yang, X., C. Zhou, W. Huo, F. Yang, X. Liu & A. Mamtimin. A study on the effects of soil moisture, air humidity, and air temperature on wind speed threshold for dust emissions in the Taklimakan Desert. Natural Hazards 97(3), 1069-1081 (2019). https://doi.org/10.1007/s11069-019-03686-1

Zan, J., B. A. Maher, X. Fang, T. Stevens, W. Ning, F. Wu, et al. Global dust impacts on biogeochemical cycles and climate. Nature Reviews Earth & Environment 6(12), 789-807 (2025). https://doi.org/10.1038/s43017-025-00734-2

Zender, C. S., H. S. Bian & D. Newman. Mineral Dust Entrainment and Deposition (DEAD) model: Description and 1990s dust climatology - art. no. 4416. Journal of Geophysical Research: Atmospheres 108(D14) (2003). https://doi.org/10.1029/2002JD002775

Zhang, M., Y. Liu, J. Zhu, Z. Wang & Z. Liu. Impact of Dust on Climate and AMOC During the Last Glacial Maximum Simulated by CESM1.2. Geophysical Research Letters 49(3), e2021GL096672 (2022). https://doi.org/https://doi.org/10.1029/2021GL096672

Zhang, Z., Y. Xue, G. M. MacDonald, P. M. Cox & G. J. Collatz. Investigation of North American vegetation variability under recent climate: A study using the SSiB4/TRIFFID biophysical/dynamic vegetation model. Journal of Geophysical Research: Atmospheres 120, 1300 - 1321 (2015).

Zhao, A., Z. Li, L. Zou, J. Wu, K. Stan & A. Sanchez-Azofeifa. Evaluating dynamic global vegetation models in China: challenges in capturing trends in leaf area and gross primary productivity. Earth Syst. Dynam. 16(6), 1935-1957 (2025). https://doi.org/10.5194/esd-16-1935-2025